BULLETIN OF THE POLISH ACADEMY OF SCIENCES
TECHNICAL SCIENCES, Vol. 69(6), 2021, Article number: e139202
DOI: 10.24425/bpasts.2021.139202

Operation of Fabry-Perot laser with nonlinear PT-symmetric mirror

Agnieszka MOSSAKOWSKA-WYSZYŃSKA[1*], **Piotr WITOŃSKI**[1], **and Paweł SZCZEPAŃSKI**[1, 2]

[1] Institute of Microelectronics and Optoelectronics, Warsaw University of Technology, ul. Koszykowa 75, 00-662 Warsaw, Poland
[2] National Institute of Telecommunications, ul. Szachowa 1, 04-894 Warsaw, Poland

Abstract. The above-threshold operation of a Fabry-Perot laser with a nonlinear PT (parity time) mirror is investigated. For the first time, the analysis accounts for gain saturation of an active medium as well as gain and loss saturation effects in the PT mirror. The obtained laser output intensity characteristics have been demonstrated as a function of various PT mirror parameters such as: the ratio of the PT structure period to laser operating wavelength, number of PT mirror primitive cells, and gain and loss saturation intensities of the PT mirror gain and loss layers. Two functional configurations of the laser have been considered: laser operating as a discrete device, and as a component of an integrated circuit. It has been shown that, in general, the laser operation depends on the PT mirror orientation with respect to the active medium of the laser. Moreover, when the laser radiation is outcoupled through the PT mirror to the free space, bistable operation is possible, when losses of the mirror's loss layer saturate faster than gain of the gain layer. Furthermore, for a given saturation intensity of the mirror loss layers, the increase of the saturation intensity of the mirror gain layers causes increasing output intensity, i.e., the PT mirror additionally amplifies the laser output signal.

Key words: lasers; integrated optics; nonlinear optics.

1. INTRODUCTION

Parity-time (PT)-symmetric structures have been investigated since the end of the last century. The elementary studies of Bender and Boettcher demonstrated that even non-Hermitian Hamiltonians can exhibit entirely real spectra as long as they meet conditions of the PT-symmetry [1]. In photonics, PT-symmetric devices are created from balanced gain and loss artificial materials. These one-dimensional nonreciprocal gratings exhibit strong amplification at the resonance wavelength [2], provide unidirectional reflective functionality [3, 4], and offer several interesting features such as nonreciprocity of light propagation and beam refraction [5, 6], or coherent perfect absorption [7].

Optical PT structures were first investigated in [8]. They are formed as periodic structures of N bilayer primitive cells. Each cell is composed of an amplifying (exhibiting gain) and absorbing (lossy) layer (for simplicity, further referred to as gain and loss layers, respectively). Their complex index of refraction along the optical z-axis should satisfy the following condition: $n^*(-z) = n(z)$, where the asterisk denotes a complex conjugate. Given that the refractive index is a complex quantity described by $n = n_R + in_I$, the PT symmetry is obtained when $n_R(z) = n_R(-z)$ and $n_I(z) = -n_I(-z)$. This implies that gain of an active layer ($n_I < 0$) and losses of an absorbing layer ($n_I > 0$) must be equal with respect to their absolute values, as long as the real parts of refractive indices are equal.

So far, a variety of applications for optical PT structures was proposed and theoretically analyzed: in lasers as a gain medium [3, 9, 10], as well as an output mirror providing intensity enhancement and concentration of the emitted beam [11] and improving power efficiency of the lasing structure [12]. The application of PT-symmetric grating in PT DFB lasers has also been theoretically studied, where a stronger modal discrimination has been observed as compared to conventional DFB lasers, enhancing performance of a single-mode operation [13].

The optical switching and bistability (and even multistability) in periodic PT-symmetric structures has been already showed in [14–16] and [17]. In the first two papers, Phang *et al*. discussed the effect of gain saturation in the PT-symmetric Bragg gratings without considering the evolution of the field amplitudes inside the primitive cell. Moreover, constant saturation in the whole investigated structure was assumed. Additionally, the authors used an assumption that only one type of a medium surrounds the PT structure. In [15–17], the Kerr nonlinearity is considered as the main cause of bistability and is stronger than the influence of the gain/loss saturation effect in the PT structure.

In this paper, the above-threshold operation of a Fabry–Perot laser with a nonlinear PT-mirror is analyzed considering gain saturation in the active medium, as well as gain/loss saturation effects in the PT-mirror. It has been shown that the interplay of the saturation effects in the active medium and PT-mirror can also lead to the bistable operation in the considered laser structure without the Kerr nonlinearity. The presented model of nonlinear laser operation is general and thus applicable to a wide range of material compositions. However, for

*e-mail: agnieszka.wyszynska@pw.edu.pl

Manuscript submitted 2021-01-13, revised 2021-06-25, initially accepted for publication 2021-09-10, published in December 2021

the purposes of numerical evaluation of the laser characteristics, typical laser parameters for structures fabricated in indium phosphide (InP) technological platform were assumed. InP does not demonstrate the Kerr nonlinearity [18] and is commonly used for fabrication of Bragg grating reflectors [19, 20], integrated photonic circuits [21], including optical telecommunication devices [22]. For such purposes, the PT mirror can be produced as a periodic grating of gain and loss layers (constituting a bilayer primitive cell of the grating), where amplification and absorption are controlled by selectively applied biasing voltage [23]. Similarly, the gain in the active medium fabricated in indium phosphide can be controlled with an external biasing.

As a result of the presented analysis, output intensity characteristics were numerically calculated for two PT laser structures, where the output laser beam is outcoupled through the PT mirror either to the free space or to the semiconductor medium. The former case corresponds to the laser structure operating as a discrete device (further referred to as a *discrete* configuration), and in the latter case the laser structure can be considered as a component of an integrated circuit (*integrated* configuration). For both cases, two different PT mirror positions are analyzed, i.e., when the loss layer of the PT mirror is faced toward the active medium (further referred to as *setup 1* – Fig. 1a) or the gain layer of the PT mirror is faced toward the active medium (further referred to as *setup 2* – Fig. 1b). For the purposes of numerical simulations, the InP refractive index of 3.165 is assumed and the laser operates at $\lambda = 1.55$ μm.

In the next section, the analysis describing transmission and reflection of the linear finite PT mirror located between an active medium and either air or a semiconductor medium is presented. The method used for the analysis of nonlinear operation of the laser with nonlinear PT mirror is also described. In Section 3, the characteristics showing reflection and transmission coefficients of the PT mirror and the output intensity of the laser are shown. Section 4 gives the conclusions.

2. THEORETICAL ANALYSIS

The laser structure under investigation, presented in Fig. 1, is composed of a Fabry–Perot resonator bounded by a classical mirror and a PT-symmetric mirror. The classical mirror amplitude coefficients of reflection and transmission are r and t, respectively, with $|r|^2 + |t|^2 = 1$ (i.e., mirror losses are neglected). The PT mirror is a periodic structure with primitive cells consisting of gain and loss layers of widths w_a and w_b, respectively, where both layers have the same width, i.e., $w_a = w_b$. Gain and absorption layers are characterized by complex refractive indices n_1 and n_2, respectively:

$$n_1 = n_{1R} - in_{1I}\,, \quad n_2 = n_{2R} + in_{2I}\,, \tag{1}$$

where $n_{1R} = n_{2R}$.

The period of the PT structure is denoted by $\Lambda = w_a + w_b$ and the length of the entire PT structure is $L^{(PT)} = N\Lambda$, where N is the number of primitive cells. The electric field complex amplitudes of waves travelling in opposite directions in gain and loss layers of the n-th PT primitive cell are denoted by $(a_n,\ b_n)$ and $(c_n,\ d_n)$, respectively, see Fig. 1.

Reflection and transmission amplitude coefficients of the PT-symmetric mirror depend on the PT mirror's orientation with respect to the active medium of the laser. Those are denoted by $r_N^{(\{\alpha,g\})}$ and $t_N^{(\{\alpha,g\})}$, respectively, where superscript (α) corresponds to setup 1, see Fig. 1a, while superscript (g) is used for setup 2, Fig. 1b. These coefficients will be calculated for linear and nonlinear PT mirror with the help of a modified transfer matrix. It is worth noting that, in contrast to a classical mirror, the energy conservation relation cannot be applied here, thus $|r_N^{(\{\alpha,g\})}|^2 + |t_N^{(\{\alpha,g\})}|^2 \neq 1$. The active medium of the laser is characterized by refractive index n_a, a normalized distributed loss coefficient $\alpha_0 L$, and a normalized small-signal gain coefficient $g_0 L$. The laser beam is outcoupled through the PT-symmetric mirror to the medium of refractive index n_s. The length of the laser cavity is equal L.

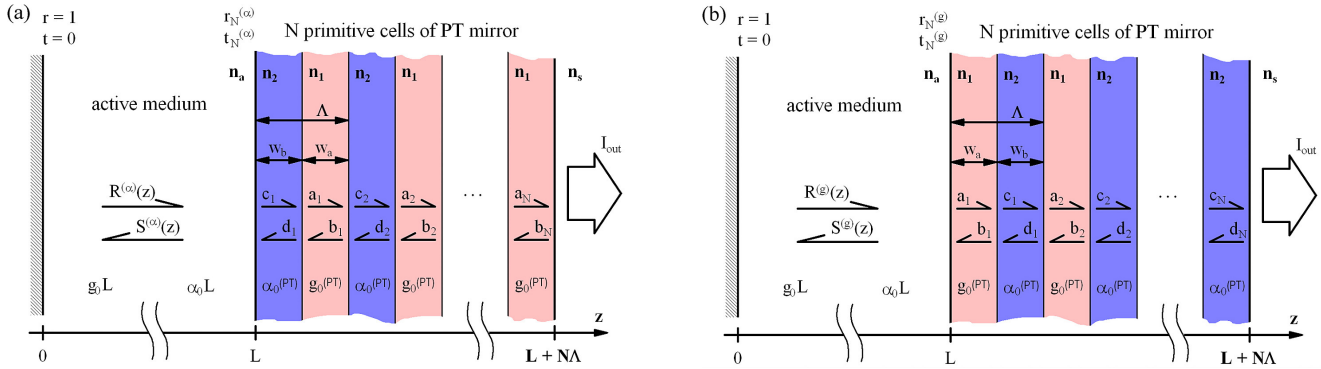

Fig. 1. Laser structure under investigation: (a) setup 1 of the laser; (b) setup 2 of the laser. List of symbols: r and t – classical mirror amplitude coefficients of reflection and transmission; L – length of laser cavity; n_a – refractive index of active medium; $\alpha_0 L$ – normalized distributed loss coefficient; $g_0 L$ – normalized small-signal gain coefficient; $R^{(\{\alpha,g\})}(z)$ and $S^{(\{\alpha,g\})}(z)$ – field amplitudes of waves incident on and reflected from PT mirror; $r_N^{(\{\alpha,g\})}$ and $t_N^{(\{\alpha,g\})}$ – reflection and transmission amplitude coefficients of PT mirror; w_a and w_b – widths of gain and loss layers; Λ – period of PT structure; N – number of PT primitive cells; $N\Lambda$ – length of PT structure; n_1 and n_2 – complex refractive indices of gain and loss layers; $g_0^{(PT)}$ and $\alpha_0^{(PT)}$ – small-signal gain and loss coefficients of PT mirror layers; $a_{1\ldots N}$ and $b_{1\ldots N}$ – electric field complex amplitudes of waves travelling in opposite directions in gain layers; $c_{1\ldots N}$ and $d_{1\ldots N}$ – electric field complex amplitudes of waves travelling in opposite directions in loss layers; n_s – refractive index of surrounding medium; I_{out} – output intensity of laser

2.1. Linear PT mirror analysis

A PT mirror linear structure is examined with the help of a modified transfer matrix method [24], where gain and loss saturation effects are neglected, and $n_{1I} = n_{2I}$. The imaginary parts of the refractive indices are related to the small-signal gain coefficient $g_0^{(PT)}$ in the mirror gain layer and to the small-signal loss coefficient $\alpha_0^{(PT)}$ in the mirror loss layer as follows:

$$n_{1I} = \left| g_0^{(PT)}/k_0 \right|, \quad n_{2I} = \left| \alpha_0^{(PT)}/k_0 \right|, \tag{2}$$

where k_0 is the wave number in free space corresponding to the lasing wavelength.

The total transfer matrices $M^{(\{\alpha,g\})}$ for a PT mirror, relating incident and output field amplitudes, also depend on its orientation with respect to the active medium. For a PT mirror consisting of a single bilayer (i.e., $N = 1$), the transfer matrices $M^{(\{\alpha,g\})}$ are:

$$M^{(\alpha)} = J_{a1} P_1 J_{12} P_2 J_{2s}\,, \tag{3a}$$

$$M^{(g)} = J_{a2} P_2 J_{21} P_1 J_{1s}\,, \tag{3b}$$

for setup 1 and setup 2, respectively. For $N > 1$, corresponding total transfer matrices can be written in the following form:

$$M^{(\alpha)} = J_{a1} \left(\prod_1^{N-1} P_1 J_{12} P_2 J_{21} \right) P_1 J_{12} P_2 J_{2s}\,, \tag{3c}$$

$$M^{(g)} = J_{a2} \left(\prod_1^{N-1} P_2 J_{21} P_1 J_{12} \right) P_2 J_{21} P_1 J_{1s}\,, \tag{3d}$$

where:

- J_{a1} and J_{a2} are matrices describing behavior of the electromagnetic wave at the boundary between the active medium of a laser and either the first PT mirror gain layer or the first PT mirror loss layer, respectively, facing the active medium;
- J_{1s} and J_{2s} matrices denote electromagnetic wave transfer through the boundary between the last PT mirror's loss layer and gain layer, respectively, and the external medium (free space or semiconductor medium);
- J_{12} and J_{21} define transfer of the electromagnetic wave through the boundary between gain and loss layer of the PT mirror, where J_{12} describes the wave transfer from gain layer to loss layer, while J_{21} defines a similar wave transfer, but in the opposite direction;
- P_1 and P_2 matrices describe the wave propagation through the PT mirror's gain and loss layer, respectively;
- the matrices J_{a1}, J_{a2}, J_{1s}, J_{2s}, J_{12} and J_{21} as well as P_1 and P_2 are defined in the Appendix, see equations (A.2)–(A.5).

Field amplitudes at the boundaries between the active medium and the PT mirror can thus be related in the following way:

$$\begin{bmatrix} R^{(\alpha)}(L) \\ S^{(\alpha)}(L) \end{bmatrix} = J_{a2} \begin{bmatrix} c_1 \\ d_1 \end{bmatrix}, \tag{4a}$$

$$\begin{bmatrix} R^{(g)}(L) \\ S^{(g)}(L) \end{bmatrix} = J_{a1} \begin{bmatrix} a_1 \\ b_1 \end{bmatrix}, \tag{4b}$$

where $R^{(\{\alpha,g\})}(L)$ and $S^{(\{\alpha,g\})}(L)$ are field amplitudes of the waves incident on and reflected from the PT mirror, respectively. a_1 and b_1 denote corresponding field amplitudes in the first PT mirror gain layer in setup 2, while c_1 and d_1 describe field amplitudes in the first loss layer in setup 1.

Similarly, relations between field amplitudes at the boundaries between the PT mirror and the surrounding medium are as follows:

$$\begin{bmatrix} c_N \\ d_N \end{bmatrix} = J_{2s} \begin{bmatrix} R_{\text{out}}^{(g)} \\ S_{\text{out}}^{(g)} \end{bmatrix}, \tag{5a}$$

$$\begin{bmatrix} a_N \\ b_N \end{bmatrix} = J_{1s} \begin{bmatrix} R_{\text{out}}^{(\alpha)} \\ S_{\text{out}}^{(\alpha)} \end{bmatrix}, \tag{5b}$$

a_N and b_N denote field amplitudes in the last PT mirror gain layer adjacent to the external medium, c_N and d_N describe field amplitudes in the last PT mirror loss layer adjacent to the external medium, and $R_{\text{out}}^{(\{\alpha,g\})}$ and $S_{\text{out}}^{(\{\alpha,g\})}$ are the corresponding output field amplitudes in the external medium.

Moreover, the amplitude reflection and transmission coefficients of the two PT-mirror can be expressed with total transfer matrix components in the following way:

$$r_N^{(\{\alpha,g\})} = \frac{M_{21}^{(\{\alpha,g\})}}{M_{11}^{(\{\alpha,g\})}}, \qquad t_N^{(\{\alpha,g\})} = \frac{1}{M_{11}^{(\{\alpha,g\})}}. \tag{6}$$

It is worth noting that transmission coefficients $t_N^{(\alpha)}$ and $t_N^{(g)}$ are equal, which is confirmed by the mirror characteristics presented in Section 3 (for additional reference and comparison, see [25]).

Finally, using components of the total transfer matrices $M^{(\{\alpha,g\})}$, it is possible to define a related scattering matrix $S^{(\{\alpha,g\})}$ in the following way:

$$\mathbf{S}^{(\{\alpha,g\})} = \begin{bmatrix} \dfrac{M_{21}^{(\{\alpha,g\})}}{M_{11}^{(\{\alpha,g\})}} & M_{21}^{(\{\alpha,g\})} - \dfrac{M_{12}^{(\{\alpha,g\})} M_{21}^{(\{\alpha,g\})}}{M_{11}^{(\{\alpha,g\})}} \\ \dfrac{1}{M_{11}^{(\{\alpha,g\})}} & \dfrac{-M_{12}^{(\{\alpha,g\})}}{M_{11}^{(\{\alpha,g\})}} \end{bmatrix}. \tag{7}$$

The eigenvalues λ_1 and λ_2 of the matrix allow to determine conditions under which the PT structure has either a PT-symmetric phase, $|\lambda_1| = |\lambda_2| = 1$, or a broken symmetry phase, $|\lambda_1| = 1/|\lambda_2|$ or $|\lambda_1| < 1$, $|\lambda_2| > 1$.

2.2. Nonlinear PT mirror analysis

The modified transfer matrix method can be also applied to investigations of nonlinear behavior of PT mirrors, where gain and loss saturation effects are taken into account. In such a case, the imaginary parts of the refractive indices evolve inside a PT mirror's primitive cell, therefore each layer of such cell is divided into narrow sublayers (see Fig. 2).

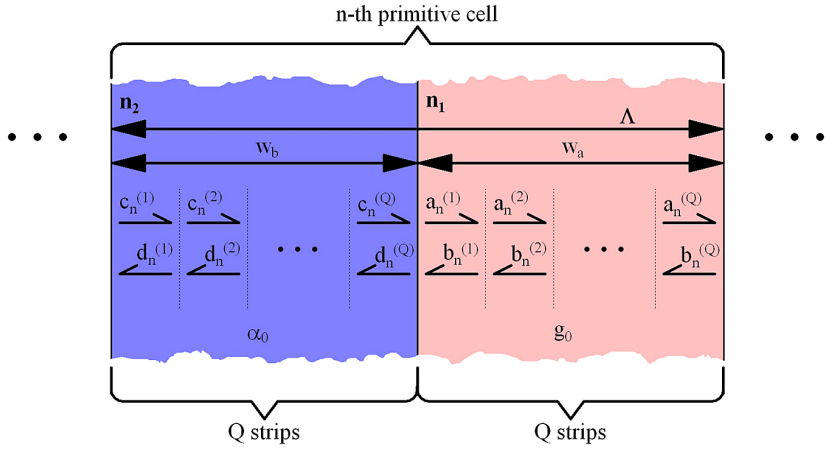

Fig. 2. Scheme of n-th primitive cell of the PT mirror divided in sublayers. List of symbols: n_1 and n_2 – complex refractive indices of gain and loss layers; Λ – period of PT structure; w_a and w_b – widths of gain and loss layers; $a_n^{(1...Q)}$ and $b_n^{(1...Q)}$ – electric field complex amplitudes of waves travelling in opposite directions in gain sublayers; $c_n^{(1...Q)}$ and $d_n^{(1...Q)}$ – electric field complex amplitudes of waves travelling in opposite directions in loss sublayers; g_0 and α_0 – small-signal gain and loss coefficients of PT mirror layers; Q – number of sublayers in gain and loss layers

In each sublayer, imaginary parts of refractive indices (with saturation effects included) can be described with the following equations [25]:

$$n_{1I}^{(i)} = \frac{\left|g_0^{(PT)}/k_0\right|}{1+\left(\left|a_n^{(i)}\right|^2+\left|b_n^{(i)}\right|^2\right)/I_{sg}}, \tag{8a}$$

$$n_{2I}^{(i)} = \frac{\left|\alpha_0^{(PT)}/k_0\right|}{1+\left(\left|c_n^{(i)}\right|^2+\left|d_n^{(i)}\right|^2\right)/I_{s\alpha}}, \tag{8b}$$

where $a_n^{(i)}$, $b_n^{(i)}$, $c_n^{(i)}$ and $d_n^{(i)}$ are the field complex amplitudes for the i-th sublayer of the n-th primitive cell (see Fig. 2). These amplitudes are normalized in such a way that the expressions $(|a_n^{(i)}|^2+|b_n^{(i)}|^2)$ and $(|c_n^{(i)}|^2+|d_n^{(i)}|^2)$ describe the power density in the related sublayer. Moreover, I_{sg} and $I_{s\alpha}$ are saturation intensities of the PT mirror gain and loss layers, respectively. Note that Q, the number of sublayers in gain and loss layers (determining the accuracy of the calculation method [25]) should be sufficiently large to justify the assumption that the imaginary part of the refractive indices is approximately constant within a single sublayer.

Complex field amplitudes in subsequent sublayers are related by elementary propagation matrices $P_1^{(i)}$ and $P_2^{(i)}$, i.e.:

$$\begin{bmatrix} a_n^{(i-1)} \\ b_n^{(i-1)} \end{bmatrix} = P_1^{(i)} \begin{bmatrix} a_n^{(i)} \\ b_n^{(i)} \end{bmatrix}, \tag{9a}$$

$$\begin{bmatrix} c_n^{(i-1)} \\ d_n^{(i-1)} \end{bmatrix} = P_2^{(i)} \begin{bmatrix} c_n^{(i)} \\ d_n^{(i)} \end{bmatrix}, \tag{9b}$$

where $P_1^{(i)}$ and $P_2^{(i)}$ are related to the imaginary parts of the refractive indices for the i-th sublayer, see equation (A.5) in the Appendix. Thus, the propagation matrices P_1 and P_2 describing the wave propagation through the PT mirror's single gain and loss layer, respectively, become a product of elementary matrices of all the sublayers, i.e.:

$$\begin{bmatrix} a_n^{(0)} \\ b_n^{(0)} \end{bmatrix} = \prod_{i=1}^{Q} P_1^{(i)} \begin{bmatrix} a_n^{(Q)} \\ b_n^{(Q)} \end{bmatrix} = P_1 \begin{bmatrix} a_n^{(Q)} \\ b_n^{(Q)} \end{bmatrix}, \tag{10a}$$

$$\begin{bmatrix} c_n^{(0)} \\ d_n^{(0)} \end{bmatrix} = \prod_{i=1}^{Q} P_2^{(i)} \begin{bmatrix} c_n^{(Q)} \\ d_n^{(Q)} \end{bmatrix} = P_2 \begin{bmatrix} c_n^{(Q)} \\ d_n^{(Q)} \end{bmatrix}, \tag{10b}$$

and the total transfer matrices $M^{(\{\alpha,g\})}$ for a nonlinear PT mirror are defined with equations (3c), (3d), with P_1 and P_2 described in equation (10). This matrix, in accordance with equation (6), also determines the mirror's transmission ($t_N^{(\alpha)}$, $t_N^{(g)}$) and reflection ($r_N^{(\alpha)}$, $r_N^{(g)}$) coefficients in the nonlinear regime.

2.3. Nonlinear laser operation

This analysis includes gain and loss saturation effects in the PT mirror along with gain saturation in the active medium. In the presented model, steady-state single mode operation is considered, and an assumption is present, that the gain line of the active medium as well as the line of gain and absorption of the PT mirror layers are homogenously broadened and the lasing wavelength is tuned to their center (or equivalently, the gain and loss linewidths are infinite). To determine the output intensity I_{out} with a PT mirror as a function of the active medium small-signal gain coefficient $g_0 L$, the following procedure scheme is proposed. In the first step, an initial value of the output field amplitude $R_{\text{out}}^{(\{\alpha,g\})}$ and the small-signal gain coefficient of the

active medium g_0L, are assumed. Moreover, to satisfy the lasing condition, the output field amplitude $S_{\text{out}}^{(\{\alpha,g\})}$ has to be zero. Next, the electric field distribution inside the PT mirror is calculated with the help of a total transfer matrix $M^{(\{\alpha,g\})}$ for a nonlinear PT mirror using equations (3a)–(3d), depending on the PT mirror orientation with respect to the gain medium, with propagation matrices P_1 and P_2 defined in equation (10). In these calculations, the intensity saturations of gain and loss layers, I_{sg} and $I_{s\alpha}$, (treated as parameters) are fixed. As a result, the electric field amplitudes $R^{(\{\alpha,g\})}(L)$ and $S^{(\{\alpha,g\})}(L)$ are obtained (see Fig. 1a and 1b). Those are the initial values required to find numerically the electric field distribution in the active nonlinear medium, whereby a similar procedure is applied as in the case of the analysis of a nonlinear PT mirror. Thus again, the active medium is divided into K narrow sublayers, each described by elementary propagation matrices $P_a^{(i)}$, see equation (A.7). Number K is sufficiently large to hold assumption that the saturated gain is constant within each sublayer. The saturation intensity I_s in the active medium is treated as a parameter.

Finally, the field amplitudes $R^{(\{\alpha,g\})}(0)$ and $S^{(\{\alpha,g\})}(0)$ on the totally reflecting classical mirror are determined by means of the output field amplitudes $R_{\text{out}}^{(\{\alpha,g\})}$ as follows:

$$\begin{bmatrix} R^{(\{\alpha,g\})}(0) \\ S^{(\{\alpha,g\})}(0) \end{bmatrix} = P_a M^{(\{\alpha,g\})} \begin{bmatrix} R_{\text{out}}^{(\{\alpha,g\})} \\ 0 \end{bmatrix}, \tag{11}$$

where P_a, being a product of $P_a^{(i)}$, is the propagation matrix describing field transfer through the whole nonlinear active medium (for explicit formula for P_a see equation (A.7)).

The procedure, which is outlined in equation (11), is repeated for the assumed output field amplitude $R_{\text{out}}^{(\{\alpha,g\})}$ until such a value of the active medium small-signal gain coefficient g_0L is found, for which the amplitudes of waves incident on and reflected from a classical mirror become equal, i.e., $R^{(\{\alpha,g\})}(0) = S^{(\{\alpha,g\})}(0)$ (since the classical mirror is totally reflecting with no phase shift assumed) fulfilling the amplitude lasing condition.

It is worth noting that the phase condition can be fulfilled by changing the position of the classical mirror by the distance no greater than half a wavelength. This shift does not remarkably affect the amplitude conditions nor the output intensity characteristic of the laser. Thus, in calculations to follow, the phase condition can be neglected, remarkably simplifying the above-threshold analysis of the laser operation, where gain and loss saturations are taken into account. In the next section, the results of numerical evaluation are discussed.

3. NUMERICAL RESULTS

First, the transmission and reflection characteristics of the linear PT mirror structure are evaluated. In this case, the gain and loss saturation effects are neglected. The calculations are performed under assumption that the real part of the refractive index is $n_R = 3.165$ and its imaginary part is $n_I = 0.1$ for the gain and loss layers of the PT structure [26].

Three sets of the grating periods Λ/λ and the minimal number of periods N, which provide maximal reflection of the PT mirror, are established. These correspond to two mirror setups as well as two laser structures considered. The sets of mirror parameters define the PT mirrors used in the nonlinear analysis and are chosen to obtain a low laser threshold. It is worth noting that, in general, the applied transfer matrix method enables analysis of a finite PT mirror placed between arbitrary media (for an approach suitable for an infinite PT grating, see, e.g., [25]).

Next, the saturation effects are taken into account in the active medium as well as in the PT mirror, and laser characteristics of the above-threshold operation are obtained. The numerical analysis is performed for the following two configurations of the laser structure. In the first configuration, the PT mirror is located between the active medium of a laser with refractive index $n_a = 3.165$ and the free space, i.e., $n_s = 1$. In this case the laser structure is a discrete device, hereinafter referred to as a discrete configuration. In the second configuration, the laser structure can be considered as a component of the integrated circuit and the corresponding refractive indices are $n_a = n_s = 3.165$. This laser structure will be referred to as an integrated configuration.

3.1. Linear PT mirror

The analysis of the linear PT mirror allows to determine its geometrical parameters, which provide the highest values of the mirror reflectivity (and hence the lowest lasing threshold). Using the modified transfer matrix method, the intensity reflection $|r_N^{(\{\alpha,g\})}|^2$ and transmission coefficients $|t_N^{(\{\alpha,g\})}|^2$ characteristics are obtained.

Figures 3 and 4 are obtained for the discrete configuration: Figs. 3(a–d) for setup 1, Figs. 4a–4d for setup 2. Figs. 3a and 3b show the intensity reflection coefficient $|r_N^{(\alpha)}|^2$ and intensity transmission coefficient $|t_N^{(\alpha)}|^2$, respectively, as functions of the number of primitive cells N, and the ratio of the grating period to the operating wavelength Λ/λ for the electro-magnetic wave incident on the mirror loss layer faced toward the active medium. In Figs. 3c and 3d, similar characteristics for $|r_N^{(g)}|^2$ and $|t_N^{(g)}|^2$ are presented for the electromagnetic wave incident on the other side of the PT mirror, i.e., on the mirror's gain layer adjacent to the free space.

The obtained characteristics of reflection and transmission coefficients show maxima for two numbers of the primitive cells, approximately equal $N \approx 20$ and $N \approx 60$ in the presented range of parameters. Periodic distribution of these maxima results from Bragg resonances [19] along the Λ/λ axis and from longitudinal distribution of the field inside the PT structure along the N axis, see the Appendix. It worth noting that the transmission coefficients are equal for both directions of the electromagnetic wave incidence. In the analysis to follow, only the PT structure with lower number N of the primitive cells, i.e., $N \approx 20$, will be considered, as a less complicated case for potential fabrication. For this case, the precisely calculated values of the intensity reflection coefficients, $|r_N^{(\alpha)}|^2$ and $|r_N^{(g)}|^2$,

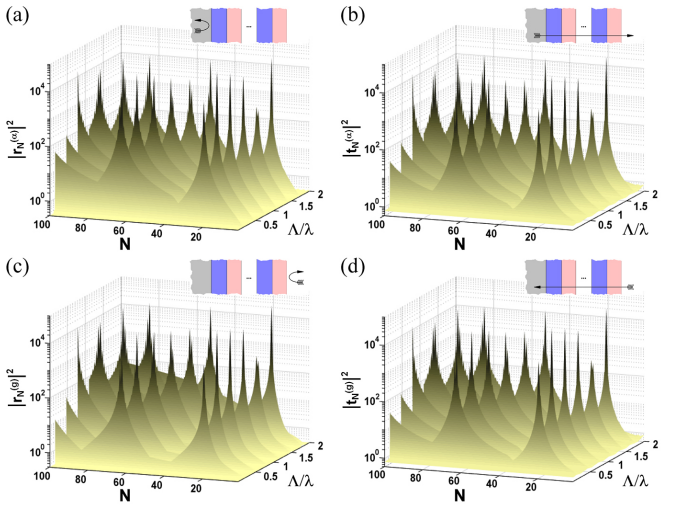

Fig. 3. Reflection $|r_N^{(\{\alpha,g\})}|^2$ and transmission $|t_N^{(\{\alpha,g\})}|^2$ coefficients of a linear PT mirror in discrete configuration for setup 1. These coefficients are plotted as a function of the number N of primitive cells and the ratio Λ/λ. In (a) and (b), the electromagnetic wave is incident on the loss layer. In (c) and (d), the electromagnetic wave is incident on the gain layer

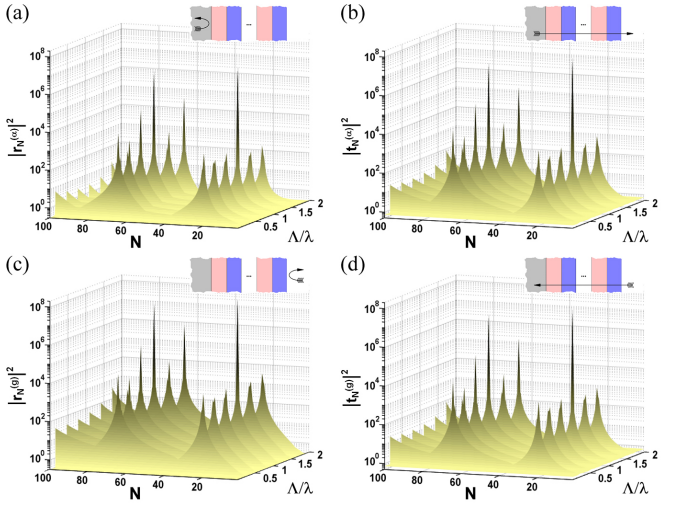

Fig. 4. Reflection $|r_N^{(\{\alpha,g\})}|^2$ and transmission $|t_N^{(\{\alpha,g\})}|^2$ coefficients of a linear PT mirror in discrete configuration for setup 2. These coefficients are plotted as a function of the number N of primitive cells and the ratio Λ/λ. In (a) and (b), the electromagnetic waveis incident on the gain layer. In (c) and (d), the electromagnetic wave is incident on the loss layer

the intensity transmission coefficients $|t_N^{(\alpha)}|^2$ and $|t_N^{(g)}|^2$, as well as the resulting mirror length $L^{(PT)}$ are shown in Table 1. The PT mirror parameters providing maximal mirror reflection (and therefore a high Q-factor of the cavity), resulting in low laser operation threshold, are highlighted. The nonlinear operation of a laser with a PT mirror so defined will be further considered.

The reflection and transmission characteristic presented in Figs. 4a–4d are repeated for setup 2 i.e., the PT mirror is reversed in comparison to the previous case. Again, in Figs. 4a and 4b, the intensity reflection and transmission coefficients, $|r_N^{(g)}|^2$ and $|t_N^{(g)}|^2$ are shown, as a function of N and Λ/λ ratio, and the electromagnetic wave is incident on the mirror gain layer faced toward the active medium, while Figs. 4c and 4d show the intensity reflection and transmission coefficients, $|r_N^{(\alpha)}|^2$ and $|t_N^{(\alpha)}|^2$ for the electromagnetic wave incident on the other side of the PT mirror, i.e., on the mirror loss layer.

Table 1

PT mirror parameters for the laser configuration as in Fig. 3

Λ/λ	N	$L^{(PT)}$ [μm]	$\lvert r_N^{(\alpha)}\rvert^2$	$\lvert r_N^{(g)}\rvert^2$	$\lvert t_N^{(\{\alpha,g\})}\rvert^2$
0.15627	22	5.33	9 049.67	3 538.67	5 611.26
0.47199	21	15.36	69 583.41	35 842.79	50 089.63
0.78770	20	24.42	37 133.55	25 341.63	30 799.26
1.10340	19	32.50	16 978.34	15 417.02	16 089.60
1.41890	17	37.39	584.13	634.02	627.19
1.41910	18	39.60	773.96	937.11	830.98
1.73450	16	43.02	27 912.16	40 115.45	33 600.65

Similarly to the previous case, the maximum of reflection $|r_N^{(g)}|^2$ obtained for the lower number N of the primitive cells, i.e., $N \approx 22$, is taken into account. For this case, the precise calculations of the PT mirror parameters are presented in Table 2, and highlighted parameters define the PT mirror structure considered further in the nonlinear analysis.

Table 2

PT mirror parameters for the laser configuration as in Fig. 4

Λ/λ	N	$L^{(PT)}$ [μm]	$\lvert r_N^{(\alpha)}\rvert^2$	$\lvert r_N^{(g)}\rvert^2$	$\lvert t_N^{(\{\alpha,g\})}\rvert^2$
0.15958	22	5.44	5792.88	1592.69	3072.62
0.47542	22	16.21	2322.14	454.44	1047.30
0.79126	22	26.98	4175.79	588.34	1591.85
1.10710	22	37.75	133673930.32	13731667.55	42846619.69
1.42300	21	46.32	3515.22	244.03	944.72
1.73880	21	56.60	5667.60	293.84	1271.27

Finally, Figs. 5a–5d present the transmission and reflection characteristics of the linear PT mirror in the integrated configuration. Because of the symmetry, it is sufficient to analyze only two cases: Figs. 5a and 5b for setup 1, Figs. 5c and 5d for setup 2. Figures 5a and 5b show the behavior of the intensity reflection coefficient $|r_N^{(\alpha)}|^2$ and intensity transmission coefficient $|t_N^{(\alpha)}|^2$, respectively, as a function of N and Λ/λ. The similar mirror characteristics are presented in Figs. 5c and 5d for $|r_N^{(g)}|^2$ and $|t_N^{(g)}|^2$, respectively, for reversed mirror structure.

Again, the maximal intensity reflections $|r_N^{(\alpha)}|^2$ and $|r_N^{(g)}|^2$ reveal a periodic dependence on the mirror primitive cell number N and the lower value of $N \approx 24$ is further considered.

Table 3 summarizes precise calculations of reflection ($|r_N^{(\alpha)}|^2$ and $|r_N^{(g)}|^2$) and transmission ($|t_N^{(\alpha)}|^2$ and $|t_N^{(g)}|^2$) coefficients, as

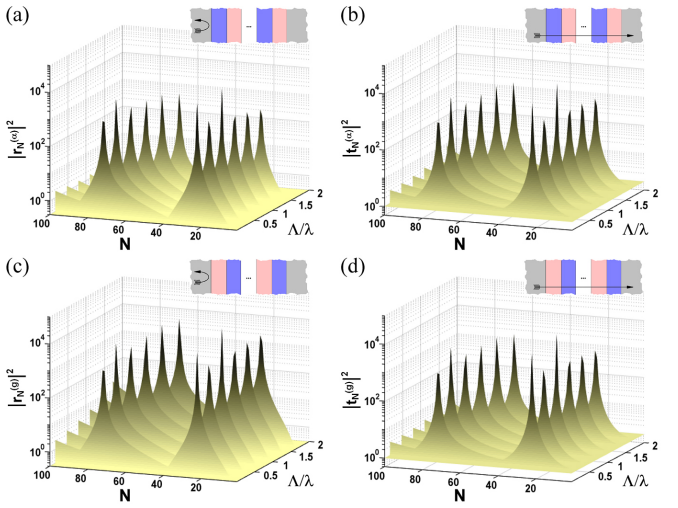

Fig. 5. Reflection $|r_N^{(\{\alpha,g\})}|^2$ and transmission $|t_N^{(\{\alpha,g\})}|^2$ coefficients of a linear PT mirror in integrated configuration. These coefficients are plotted as a function of N and Λ/λ for setup 1 in (a) and (b), for setup 2 in (c) and (d)

Table 3
PT mirror parameters for the laser configuration as in Fig. 5

Λ/λ	N	$L^{(PT)}$ [μm]	$\lvert r_N^{(\alpha)}\rvert^2$	$\lvert r_N^{(g)}\rvert^2$	$\lvert t_N^{(\{\alpha,g\})}\rvert^2$
0.15798	25	6.12	8365.52	10202.46	9239.96
0.47393	25	18.36	1097.62	1991.77	1479.59
0.78989	24	29.38	10061.27	27161.85	16532.26
1.10580	23	39.42	581.44	2335.12	1166.27
1.42180	23	50.69	468.56	2799.96	1146.39
1.73780	22	59.26	341.44	3034.97	1019.09

well as the PT mirror length $L^{(PT)}$ for Λ/λ and N corresponding to the chosen peak of reflection.

Moreover, for the chosen mirror parameters highlighted in Tables 1–3, the symmetry of the PT mirror is investigated. For this purpose, the calculation of the eigenvalues λ_1 and λ_2 of the $\boldsymbol{S}^{(\{\alpha,g\})}$ matrix, defined in equation (7), has been performed. In general, the PT mirror meets the conditions for PT-symmetry when the eigenvalues λ_1 and λ_2 are unimodular (i.e., satisfy the condition $|\lambda_1| = |\lambda_2| = 1$). On the other hand, it has a broken symmetry phase, when $|\lambda_1| = 1/|\lambda_2|$ and $|\lambda_1| < 1$ or $|\lambda_2| > 1$ [19]. The results obtained are illustrated in Figs. 6a–6f, where the eigenvalues $|\lambda_1|$ and $|\lambda_2|$ are plotted versus Λ/λ for the primitive cell number N highlighted in Tables 1–3, respectively. The figures presented in the right column, i.e., Figs. 5b, 5d, and 5f, show more precisely the behavior of the eigenvalue highest maxima observed in the corresponding figures presented in the left column, i.e., in Figs. 5a, 5c, and 5f, respectively. These maxima of $|\lambda_1|$ and $|\lambda_2|$ shown in Figs. 5a and 5b, Figs. 5c and 5d, and Figs. 5e and 5f correspond to the reflection and transmission coefficients highlighted in Table 1, Table 2, and in Table 3, respectively.

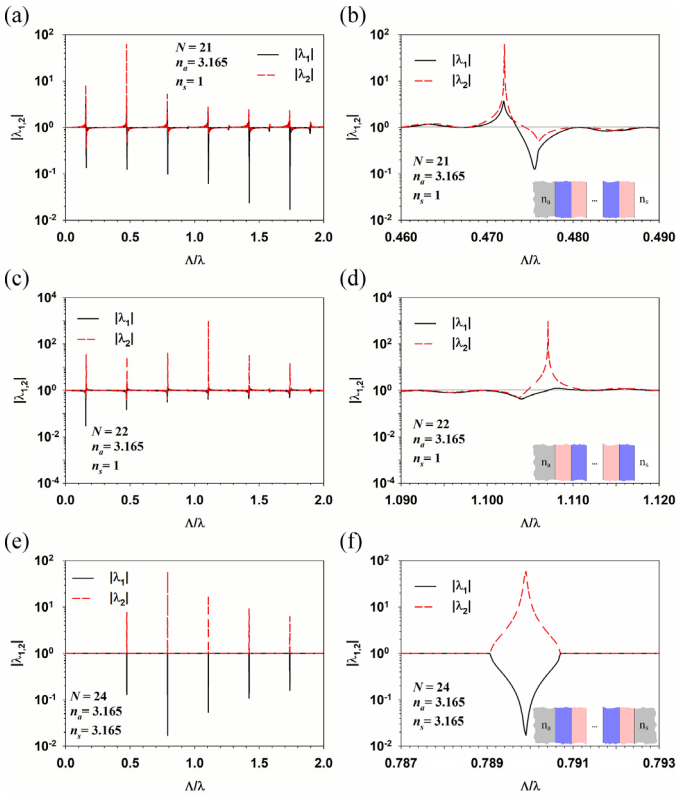

Fig. 6. Eigenvalues λ_1, λ_2 shown as a function of ratio Λ/λ for PT mirror structures. Figures on the right side show more precisely the behavior of the eigenvalue highest maxima observed in the corresponding figures presented on the left side. Figsures (a)–(d) characteristics are plotted for a PT mirror in discrete configuration (a) and (b) for setup 1 and parameters highlighted in Table 1; (c) and (d) for setup 2 and parameters highlighted in Table 2. Figures (e) and (f) show characteristics for the PT mirror in integrated configuration of a laser for parameters highlighted in Table 3

As can be noticed, for the PT mirror located between the active medium (i.e., semiconductor) and the free space, none of the symmetry conditions is met for the mirror parameters highlighted in Table 1. Such situation is observed in Figs. 6a and 6b ($\Lambda/\lambda = 0.4720$, $N = 21$) for setup 1, and in Fig. 6c and 6d ($\Lambda/\lambda = 1.1071$, $N = 22$) for setup 2, where the PT mirror is reversed. Thus, in this case, the PT mirror providing high cavity Q-factor loses its PT symmetry.

A different situation is observed for the PT mirror structure located between the active medium and the semiconductor medium, see Figs. 6e and 6f. This structure meets the conditions of a broken symmetry phase for the reflection and transmission maxima obtained for mirror parameters highlighted in Table 3 ($\Lambda/\lambda = 0.7899$, $N = 24$).

In the next section, the nonlinear operation a laser with a PT structure as an output mirror, defined by the parameters highlighted in Tables 1–3, is analyzed.

3.2. Laser with nonlinear PT mirror

This analysis includes gain and loss saturation effects in the PT mirror along with gain saturation in the active medium. In the presented model, single mode operation is considered,

and an assumption is present, that the gain line of the active medium as well as the line of gain and absorption of the PT mirror layers are homogenously broadened and the lasing wavelength is tuned to their center (or equivalently, the gain and loss linewidths are infinite).

The investigated laser with a nonlinear PT mirror is shown in Fig. 1. The numerical evaluation of the output intensity $I_{\text{out}}^{(\{\alpha,g\})} = |R_{\text{out}}^{(\{\alpha,g\})}|^2$ is performed for the discrete and integrated configuration. The following parameters of the laser structure are assumed: the classical mirror of the resonator is totally reflective, $|r|^2 = 1$, and provides no phase shift; the PT mirror is defined by the mirror parameters highlighted in Tables 1–3, the active medium distributed loss coefficient normalized to the length of the resonator is $\alpha_0 L = 0.01$, and the saturation intensity of the active medium equals $I_s = 10^3$ W/cm^2, which is a realistic value for an InP laser structure [27].

All the laser characteristics presented in Figs. 7 are plotted for the laser structure in discrete configuration. In this case, for the assumed PT mirror parameters, it does not reveal any PT-symmetry conditions. They show the dependence of the output intensity $I_{\text{out}}^{(\{\alpha,g\})}$ as a function of the normalized small-signal gain coefficient $g_0 L$ for various saturation intensities $I_{s\alpha}$ and I_{sg} of the PT mirror loss and gain layers, respectively. In is worth noting that the assumed range of saturation parameters $I_{s\alpha}$ and I_{sg} used for calculations is also realistic and available in InP active and passive structures [28]. The characteristics presented in the left column, i.e., Figs. 7a, 7c, 7e, and 7g, showing the dependence of $I_{\text{out}}^{(\alpha)}$ on $g_0 L$ for various $I_{s\alpha}$ and I_{sg}, are obtained for setup 1 of a laser, while in the right column Figs. 7b, 7d, and 7h, illustrate the behavior of $I_{\text{out}}^{(g)}$ for the reversed PT mirror structure, i.e., setup 2. Moreover, the characteristics in the left column and in the right column are obtained for the PT-mirror parameters highlighted in Table 1 and Table 2, respectively.

In general, as can be noticed, the output intensity increases with an increasing gain coefficient $g_0 L$. Such behavior is observed for a classical F-P laser when an increase of the pumping level causes an increasing output intensity.

For a lower pumping level of the active medium, i.e., smaller values of $g_0 L$, the dependence of $I_{\text{out}}^{(\{\alpha,g\})}$ on $g_0 L$ is determined considering the active medium gain saturation and the mutual relation between the saturation intensity levels of gain and losses in the gain and loss layers of the PT mirror.

For setup 1, when the mirror gain layer is an output of the whole laser structure (the characteristics in the left column of Fig. 7), the output intensity is greater than for the opposite orientation of the PT mirror (the characteristics in the right column of Fig. 7). It is caused by the fact that the PT mirror orientation significantly affects the output intensity level.

In general, in Figs. 7a–7f, for a given saturation intensity of the mirror loss layers $I_{s\alpha}$, the increase of the saturation intensity of the mirror gain layers I_{sg} causes increasing output intensity. This is the result of an increasing involvement of the PT mirror in the amplification process of the whole laser. Moreover, it is worth noting that, for a given I_{sg}, the increase of $I_{s\alpha}$ results in a decreasing output intensity and decreasing involvement of the PT mirror in the amplification process.

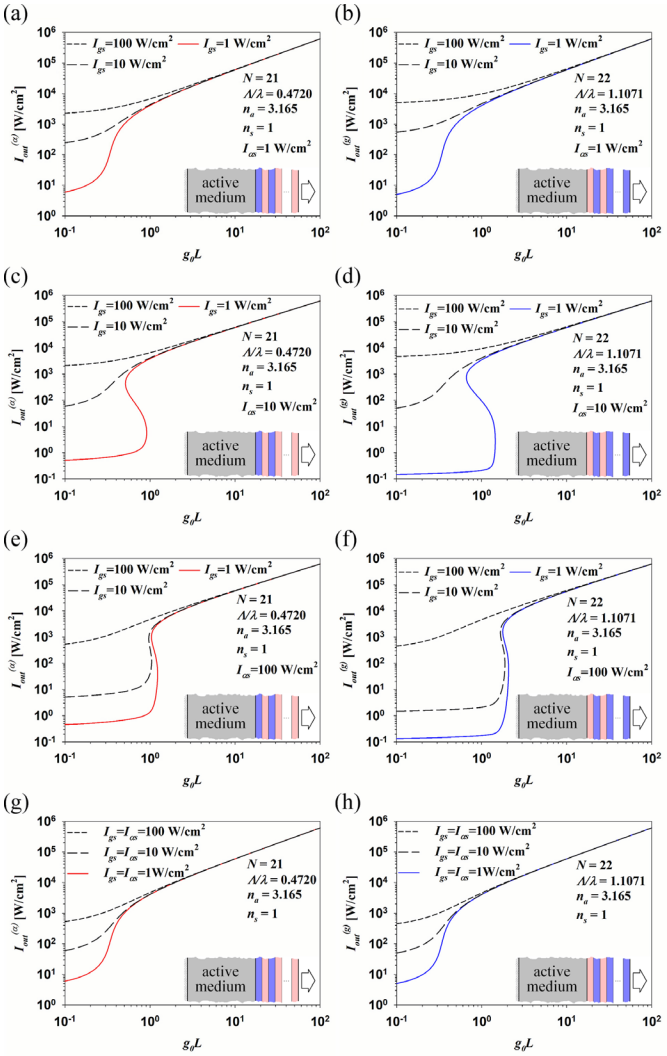

Fig. 7. Output intensity $I_{\text{out}}^{(\{\alpha,g\})}$ of the laser in discrete configuration, plotted as a function of normalized small-signal gain coefficient $g_0 L$ for various loss $I_{s\alpha}$ and gain I_{sg} saturation intensities of the mirror loss and gain layers: (a) and (b) $I_{s\alpha} = 1$ W/cm^2 and $I_{sg} = 1$, 10, 100 W/cm^2; (c) and (d) $I_{s\alpha} = 10$ W/cm^2 and $I_{sg} = 1$, 10, 100 W/cm^2; (e) and (f) $I_{s\alpha} = 100$ W/cm^2 and $I_{sg} = 1$, 10, 100 W/cm^2; (g) and (h) $I_{sg} = I_{s\alpha} = 1$, 10, 100 W/cm^2. Characteristics in the left column – for setup 1, right column – setup 2

As can be noticed in Figs. 7c–7f, when the saturation intensity of the mirror loss layers $I_{s\alpha}$ is greater than the saturation intensity I_{sg} of the mirror gain layers, and both are lower than the active medium gain saturation I_s, a bistable operation of the laser takes place. In this case, the PT mirror acts as a saturable absorber since the PT mirror loss layers saturate more slowly than the gain layers and the PT mirror provides an additional net loss to the laser structure. As a result, the hysteresis loops in the output intensity characteristic appear.

In the case where the saturation intensities of the mirror gain and loss layers are equal, i.e., $I_{s\alpha} = I_{sg}$, see Figs. 7g and 7h, the output intensity increases together with an increase in both saturation intensities. Such behavior is similar as in a classical F-P laser because the increase of the saturation intensity I_{sg} causes

an increased output intensity. Moreover, for small pumping levels (i.e., smaller values of g_0L), the difference between output intensity characteristics are smaller than for characteristics in Figs. 7a–7f.

In Figs. 7a–7h, for large values of gain coefficient g_0L, the output intensity characteristics $I_{\text{out}}^{(\{\alpha,g\})}$ tend to overlap, regardless of the setup, or the gain and loss saturation levels in the PT mirror. In this regime, the PT mirror becomes linear, since the generated laser beam intensity is high enough to saturate gain and losses in the PT mirror layers (for the assumed range of $I_{s\alpha}$ and I_{sg}).

All the characteristics presented in Figs. 8a–8h, for the laser in integrated configuration, show the dependence of the output intensity $I_{\text{out}}^{(\{\alpha,g\})}$ as a function of the normalized small-signal gain coefficient g_0L for various saturation intensities $I_{s\alpha}$ and I_{sg} of the PT mirror loss and gain layers, respectively. In this case, the PT mirror is defined using parameters highlighted in Table 3 and the conditions of a broken PT-symmetry phase are fulfilled. Again, the figures presented in the left column, i.e., Figs. 8a, 8c, 8e, and 8g, are obtained for setup 1 while in the right column, i.e., Figs. 8b, 8d, 8f, and 8h, for the reverse mirror structure, i.e., setup 2.

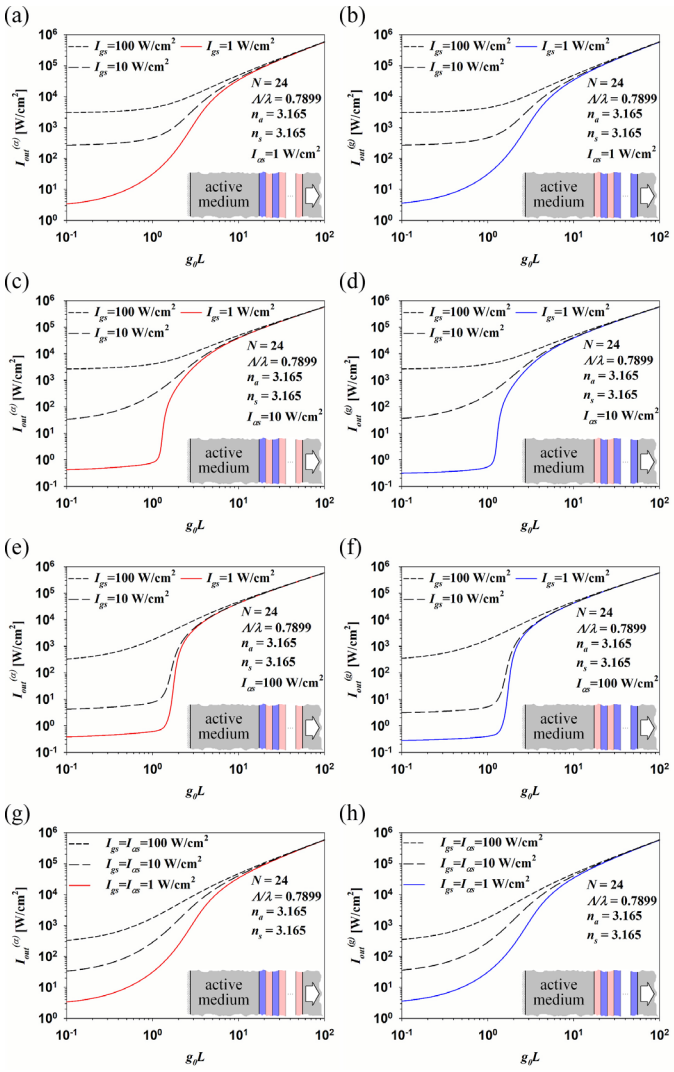

Fig. 8. Output intensity $I_{\text{out}}^{(\{\alpha,g\})}$ of the integrated configuration, plotted as a function of normalized small-signal gain coefficient g_0L for various loss $I_{s\alpha}$ and gain I_{sg} saturation intensities of the mirror loss and gain layers: (a) and (b) $I_{s\alpha}$ = 1 W/cm^2 and I_{sg} = 1, 10, 100 W/cm^2; (c) and (d) $I_{s\alpha}$ = 10 W/cm^2 and I_{sg} = 1, 10, 100 W/cm^2; (e) and (f) $I_{s\alpha}$ = 100 W/cm^2 and I_{sg} = 1, 10, 100 W/cm^2; (g) and (h) $I_{sg} = I_{s\alpha}$ = 1, 10, 100 W/cm^2. Characteristics in the left column – for setup 1, right column – setup 2

Behavior of characteristics in Fig. 8, due to the change of the saturation intensities $I_{s\alpha}$ and I_{sg}, is likewise as in Fig. 7. Similarly, the output intensity $I_{\text{out}}^{(\{\alpha,g\})}$ increases with an increasing normalized small-signal gain coefficient g_0L; for a given saturation intensity $I_{s\alpha}$, an increase of the saturation intensity I_{sg} causes an increasing output intensity; for a given saturation intensity I_{sg}, an increase of the saturation intensity $I_{s\alpha}$ causes a decreasing output intensity.

Moreover, the influence of the PT mirror orientation on the output intensity value is negligibly small and does not affect the output intensity level. Thus, the laser characteristics on the left and right column almost overlap.

It is worth noting, that bistable behavior is not observed in such a laser configuration, where the output laser beam is outcoupled through the PT mirror to the semiconductor medium. This is caused by a small difference in refractive indices of a semiconductor medium and the PT mirror. Moreover, in this case, the nonreciprocal response is not present.

Additionally, the value of the normalized small-signal gain coefficient g_0L, with which the laser characteristics begin to overlap, is greater than that for the characteristics in Fig. 7. Such behavior is caused by a small difference in refractive indices between the PT mirror and the surrounding media. It results in decreasing electromagnetic field intensity inside the mirror and increasing gain coefficient g_0L, for which the PT mirror gain, and loss layers start to saturate.

4. CONCLUSIONS

This work shows the output intensity of a laser with a PT-symmetric mirroring structure, as a function of the normalized small-signal gain coefficient for the ratio of the PT structure period to the laser operating wavelength and the number of primitive cells constituting PT mirror, treated as parameters. The linear analysis of the PT mirror allowed to select such PT structure's geometrical parameters, which were used in the design of the PT laser structure operating as discrete device as well as a component of an integrated circuit. Considering gain and loss saturation effects, the modified transfer matrix method was applied to obtain the relationship between the output intensity and the gain coefficient.

As a result of the nonlinear analysis, the output intensity characteristics were numerically calculated for two configurations of the PT laser structures, where the output laser beam was coupled either to the free space or to the semiconductor medium. All the presented characteristics increased with increasing normalized small-signal gain coefficient (i.e., for higher pumping levels) and tended to overlap for large values of the gain coefficient, regardless of the type of the PT layer facing

the active medium. Moreover, all the characteristics strongly depend on the gain and loss saturation intensities levels in the PT mirror. For a given saturation intensity of the mirror loss layers $I_{s\alpha}$, the increase of the saturation intensity of the mirror gain layers I_{sg} causes increasing output intensity of the overall laser structure. In this case, the PT mirror acts as an additional amplifier.

The obtained laser characteristics showed bistable behavior only when (1) the output laser beam was coupled to the free space (i.e., the laser operates as a discrete device and the PT mirror is placed between two media of remarkably different refractive indices), (2) the loss layer saturation intensity was greater than gain layer saturation intensity, but smaller than the active medium saturation intensity (i.e., the losses of the loss layer saturate faster than the gain of the gain layer), and (3) the output laser beam left the laser structure through the loss or gain mirror layer.

The model proposed in this paper can be useful for modeling laser structures with a PT mirror. Investigation of such PT structures may open doors to next-generation laser sources for telecommunication systems and optical computing.

A. APPENDIX

The electric field distribution inside the primitive cell of the PT mirror is expressed as a sum of two counter-running plane waves along the z direction:

$$E_1(z) = a_n e^{ik_0 n_1 z} + b_n e^{-ik_0 n_1 z}. \tag{A.1a}$$

$$E_2(z) = c_n e^{ik_0 n_2 z} + d_n e^{-ik_0 n_2 z}. \tag{A.1b}$$

The junction matrices J_{a1} and J_{a2} describing transfer of the electromagnetic wave from the active medium with refractive index n_a to the first PT mirror gain and loss layer of refractive indices n_1 and n_2 respectively, are of the following form:

$$J_{a\{1,2\}} = \begin{bmatrix} \dfrac{n_a + n_{\{1,2\}}}{2n_a} & \dfrac{n_a - n_{\{1,2\}}}{2n_a} \\ \dfrac{n_a - n_{\{1,2\}}}{2n_a} & \dfrac{n_a + n_{\{1,2\}}}{2n_a} \end{bmatrix}. \tag{A.2}$$

The matrices J_{1s} and J_{2s}, defining transfer of the electromagnetic wave from the last PT mirror gain or loss layer of refractive indices n_1 and n_2, respectively, to the free space or the semiconductor medium, respectively, of refractive index n_s, are as follows:

$$J_{\{1,2\}s} = \begin{bmatrix} \dfrac{n_{\{1,2\}} + n_s}{2n_{\{1,2\}}} & \dfrac{n_{\{1,2\}} - n_s}{2n_{\{1,2\}}} \\ \dfrac{n_{\{1,2\}} - n_s}{2n_{\{1,2\}}} & \dfrac{n_{\{1,2\}} + n_s}{2n_{\{1,2\}}} \end{bmatrix}. \tag{A.3}$$

Matrix J_{12} express transfer of the electromagnetic wave from the gain (with the refractive index n_1) to the loss layer (with the refractive index n_2) of the PT structure, while matrix J_{21} defines a similar electromagnetic wave transfer in the opposite direction:

$$J_{\{12,21\}} = \begin{bmatrix} \dfrac{n_{\{1,2\}} + n_{\{2,1\}}}{2n_{\{1,2\}}} & \dfrac{n_{\{1,2\}} - n_{\{2,1\}}}{2n_{\{1,2\}}} \\ \dfrac{n_{\{1,2\}} - n_{\{2,1\}}}{2n_{\{1,2\}}} & \dfrac{n_{\{1,2\}} + n_{\{2,1\}}}{2n_{\{1,2\}}} \end{bmatrix}. \tag{A.4}$$

Propagation matrices P_1 and P_2 describe transfer of the electromagnetic wave through the PT mirror gain (with the refractive index n_1) and loss (with the refractive index n_2) layer, respectively, as follows:

$$P_{\{1,2\}} = \begin{bmatrix} e^{-ik_0 n_{\{1,2\}} w_{\{a,b\}}} & 0 \\ 0 & e^{ik_0 n_{\{1,2\}} w_{\{a,b\}}} \end{bmatrix}. \tag{A.5}$$

In the case of a nonlinear PT mirror, the elementary matrix $P_1^{(i)}$ of the i-th sublayer of the gain layer with complex refractive index defined in equation (A.5a) and the elementary matrix $P_2^{(i)}$ of the i-th sublayer of the loss layer with complex refractive index defined in equation (A.5b), have the following form:

$$P_1^{(i)} = \begin{bmatrix} e^{-ik_0\left(n_{1R} - in_{1I}^{(i)}\right)\frac{w_a}{Q}} & 0 \\ 0 & e^{ik_0\left(n_{1R} - in_{1I}^{(i)}\right)\frac{w_a}{Q}} \end{bmatrix}, \tag{A.6a}$$

$$P_2^{(i)} = \begin{bmatrix} e^{-ik_0\left(n_{2R} + in_{2I}^{(i)}\right)\frac{w_b}{Q}} & 0 \\ 0 & e^{ik_0\left(n_{2R} + in_{2I}^{(i)}\right)\frac{w_b}{Q}} \end{bmatrix}. \tag{A.6b}$$

The transfer matrix method is also used to describe wave propagation in the active medium. For such medium, the propagation matrix P_a is expressed as:

$$\begin{aligned} P_a &= \prod_{i=1}^{K} P_a^{(i)} \\ &= \prod_{i=1}^{K} \begin{bmatrix} e^{-ik_0\left(n_a + i\frac{\alpha_0 - g^{(i)}}{k_0}\right)\frac{L}{K}} & 0 \\ 0 & e^{ik_0\left(n_a + i\frac{\alpha_0 - g^{(i)}}{k_0}\right)\frac{L}{K}} \end{bmatrix}, \end{aligned} \tag{A.7}$$

where the saturated gain in the active medium is described as:

$$g^{(i)} = \frac{g_0}{1 + \left(\left|R^{(\{\alpha,g\})(i)}\right|^2 + \left|S^{(\{\alpha,g\})(i)}\right|^2\right)/I_s},$$

$R^{(\{\alpha,g\})(i)}$ and $S^{(\{\alpha,g\})(i)}$ are the electric longitudinal field's complex amplitudes travelling in opposite directions in the active medium of the laser.

The following figure shows two examples of the longitudinal field distribution of counter running waves in the PT structure (discrete configuration for setup 1) as a function of the number of primitive cells N. First plot, shown in Fig. 9a, is obtained for the PT structure parameters highlighted in Table 1, providing maximal mirror reflection and transmission coefficients (see Fig. 3). Second plot, Fig. 9b, is drawn for $\Lambda/\lambda = 0.62985$, the

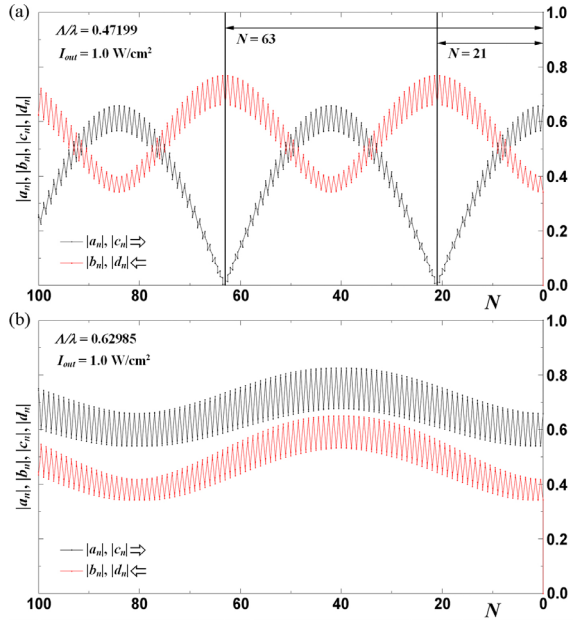

Fig. 9. Longitudinal field distribution of counter running waves $|a_n|$, $|b_n|$, $|c_n|$, $|d_n|$, inside the linear PT mirror structure in discrete configuration for setup 1, as a function of the number of primitive cells N for $I_{\text{out}} = 1$ W/cm^2 and (a) $\Lambda/\lambda = 0.47199$, (b) $\Lambda/\lambda = 0.62985$

value between two neighboring maxima in Table 1 (second and third row), resulting in the mirror reflection and transmission coefficients lower than unity.

As can be seen, the longitudinal field distribution shown in Fig. 9 is a periodic function of N. This distribution affects the values of reflection and transmission coefficients. In Fig. 9a, for marked $N = 21$ and $N = 63$, the amplitude of right travelling wave reaches minima, and left travelling – maxima, which corresponds to the maximum values of reflections and transmissions coefficients (see Fig. 3). Comparing with the previous case, in Fig. 9b, the amplitudes of travelling waves change slightly with the value of N, and therefore the reflection and transmission coefficients are very low.

ACKNOWLEDGEMENTS

In particular, the authors wish to thank Mr. Marcin Kieliszczyk for checking linguistic correctness of the manuscript.

REFERENCES

[1] C.M. Bender and S. Boettcher, "Real Spectra in Non-Hermitian Hamiltonians Having PT Symmetry," *Phys. Rev. Lett.*, vol. 80, no. 24, pp. 5243–5246, Jun. 1998, doi: 10.1103/PhysRevLett.80.5243.

[2] M. Kulishov, J.M. Laniel, N. Bélanger, J. Azaña, and D.V. Plant, "Nonreciprocal waveguide Bragg gratings," *Opt. Express*, vol. 13, no. 8, pp. 3068–3078, Apr. 2005, doi: 10.1364/OPEX.13.003068.

[3] M. Kulishov, B. Kress, and H.F. Jones, "Novel optical characteristics of a Fabry-Perot resonator with embedded PT-symmetrical grating," *Opt. Express*, vol. 22, no. 19, pp. 23164–23181, Sep. 2014, doi: 10.1364/OE.22.023164.

[4] Z. Lin, H. Ramezani, T. Eichelkraut, T. Kottos, H. Cao, and D.N. Christodoulides, "Unidirectional Invisibility Induced by PT-Symmetric Periodic Structures," *Phys. Rev. Lett.*, vol. 106, no. 21, p. 213901, May 2011, doi: 10.1103/PhysRevLett.106.213901.

[5] K.G. Makris, R. El-Ganainy, D.N. Christodoulides, and Z.H. Musslimani, "Beam Dynamics in PT Symmetric Optical Lattices," *Phys. Rev. Lett.*, vol. 100, no. 10, p. 103904, Mar. 2008, doi: 10.1103/PhysRevLett.100.103904.

[6] M.C. Zheng, D.N. Christodoulides, R. Fleischmann, and T. Kottos, "PT optical lattices and universality in beam dynamics," *Phys. Rev. A*, vol. 82, no. 1, p. 010103, Jul. 2010, doi: 10.1103/PhysRevA.82.010103.

[7] Y. Sun, W. Tan, H. Li, J. Li, and H. Chen, "Experimental Demonstration of a Coherent Perfect Absorber with PT Phase Transition," *Phys. Rev. Lett.*, vol. 112, no. 14, p. 143903, Apr. 2014, doi: 10.1103/PhysRevLett.112.143903.

[8] R. El-Ganainy, K.G. Makris, D.N. Christodoulides, and Z.H. Musslimani, "Theory of coupled optical PT-symmetric structures," *Opt. Lett.*, vol. 32, no. 17, pp. 2632–2634, Sep. 2007, doi: 10.1364/OL.32.002632.

[9] L. Ge and R. El-Ganainy, "Nonlinear Modal Interactions in PT-Symmetric Lasers," in *Frontiers in Optics 2016,* 2016, p. JW4A.186, doi: 10.1364/FIO.2016.JW4A.186.

[10] Z. Feng, J. Ma, Z. Yu, and X. Sun, "Circular Bragg lasers with radial PT symmetry: design and analysis with a coupled-mode approach," *Photonics Res.*, vol. 6, no. 5, pp. A38–A42, May 2018, doi: 10.1364/PRJ.6.000A38.

[11] M. Botey, W.W. Ahmed, J. Medina, R. Herrero, and K. Staliunas, "Non-Hermitian Broad Aperture Semiconductor Lasers Based on PT-Symmetry," in *21st International Conference on Transparent Optical Networks (ICTON 2019),* 2019, pp. 1–4, doi: 10.1109/ICTON.2019.8840291.

[12] A. Mossakowska-Wyszyńska, P. Niedźwiedziuk, P. Witoński, and P. Szczepański, "Analysis of Light Generation in Laser with PT-Symmetric Mirror," in *Advanced Photonics 2018 (BGPP, IPR, NP, NOMA, Sensors, Networks, SPPCom, SOF),* 2018, p. JTu5A.50, doi: 10.1364/BGPPM.2018.JTu5A.50.

[13] Y. Zhu, Y. Zhao, J. Fan, and L. Zhu, "Modal Gain Analysis of Parity-Time-Symmetric Distributed Feedback Lasers," *IEEE J. Sel. Top. Quantum Electron.*, vol. 22, no. 5, pp. 5–11, Sep. 2016, doi: 10.1109/JSTQE.2016.2537209.

[14] S. Phang, A. Vukovic, H. Susanto, T.M. Benson, and P. Sewell, "Ultrafast optical switching using parity–time symmetric Bragg gratings," *J. Opt. Soc. Am. B*, vol. 30, no. 11, pp. 2984–2991, 2013, doi: 10.1364/JOSAB.30.002984.

[15] S. Phang, A. Vukovic, H. Susanto, T. M. Benson, and P. Sewell, "Impact of dispersive and saturable gain/loss on bistability of nonlinear parity–time Bragg gratings," *Opt. Lett.*, vol. 39, no. 9, pp. 2603–2606, May 2014, doi: 10.1364/OL.39.002603.

[16] J. Liu, X.-T. Xie, C.-J. Shan, T.-K. Liu, R.-K. Lee, and Y. Wu, "Optical bistability in nonlinear periodical structures with PT-symmetric potential," *Laser Phys.*, vol. 25, no. 1, p. 015102, 2015, doi: 10.1088/1054-660X/25/1/015102.

[17] K. Mukherjee and P.C. Jana, "Controlled optical bistability in parity-time-symmetric coupled micro-cavities: Possibility of all-optical switching," *Physica E Low Dimens. Syst. Nanostruct.*, vol. 117, p. 113780, Mar. 2020, doi: 10.1016/j.physe.2019.113780.

[18] D.R. Paschotta, "Pockels Effect," [Online]. Available: www.rp-photonics.com/pockels_effect.html. [Accessed: 11. Dec. 2020].

[19] M. Kamp, J. Hofmann, A. Forchel, and S. Lourdudoss, "Ultrashort InGaAsP/InP lasers with deeply etched Bragg mirrors," *Appl. Phys. Lett.*, vol. 78, no. 26, pp. 4074–4075, Jun. 2001, doi: 10.1063/1.1377623.

[20] M. Happach, *et al*., "Temperature-Tolerant Wavelength-Setting and -Stabilization in a Polymer-Based Tunable DBR Laser," *J. Light. Technol.*, vol. 35, no. 10, pp. 1797–1802, May 2017, doi: 10.1109/JLT.2017.2652223.

[21] M. Smit, K. Williams, and J. van der Tol, "Past, present, and future of InP-based photonic integration," *APL Photonics*, vol. 4, no. 5, p. 050901, May 2019, doi: 10.1063/1.5087862.

[22] F.M. Soares, M. Baier, T. Gaertner, N. Grote, M. Moehrle, T. Beckerwerth, P. Runge, and M. Schell, "InP-Based Foundry PICs for Optical Interconnects," *Appl. Sci.*, vol. 9, no. 8, p. 1588, Apr. 2019, doi: 10.3390/app9081588.

[23] NeoPhotonics Corporation, "Indium Phosphide PICs," [Online]. Available: www.neophotonics.com/technology/indium-phosphide-pics/. [Accessed: 23. May 2019].

[24] S. Phang, *Theory and numerical modelling of parity-time symmetric structures for photonics*, PhD thesis, University of Nottingham, 15 Jul. 2016. [Online]. Available: eprints.nottingham.ac.uk/32596/ [Accessed: 30. Nov. 2018]

[25] P. Witoński, A. Mossakowska-Wyszyńska, and P. Szczepański, "Effect of Nonlinear Loss and Gain in Multilayer PT-Symmetric Bragg Grating," *IEEE J. Quantum Electron.*, vol. 53, no. 6, pp. 1–11, Dec. 2017, doi: 10.1109/JQE.2017.2761380.

[26] O.V. Shramkova and G.P. Tsironis, "Resonant Combinatorial Frequency Generation Induced by a PT-Symmetric Periodic Layered Stack," *IEEE J. Sel. Top. QE.,* vol. 22, no. 5, p. 5000307, Sep./Oct. 2016, doi: 10.1109/JSTQE.2015.2505139.

[27] H. Haug and L. Banyai, Red., *Optical Switching in Low-Dimensional Systems*. Plenum Press, New York, Springer US, 1989, pp. 35–48.

[28] E. Garmire and A. Kost, Red., *Nonlinear Optics in Semiconductors I: Nonlinear Optics in Semiconductor Physics I*, 1st edition. Academic Press US, 1998, pp. 364–371.